JACS Au
AN OPEN ACCESS JOURNAL OF THE AMERICAN CHEMICAL SOCIETY

pubs.acs.org/jacsau
Perspective

Structure-Guided Approaches for Enhanced Spin-Splitting in Chiral Perovskite

Zijin Ding, Quanlin Chen, Yuanzhi Jiang, and Mingjian Yuan*

Cite This: *JACS Au* 2024, 4, 1263−1277

ABSTRACT: Hybrid organic−inorganic perovskites with diverse lattice structures and chemical composition provide an ideal material platform for novel functionalization, including chirality transfer. Chiral perovskites combine organic and inorganic sublattices, therefore encoding the structural asymmetry into the electronic structures and giving rise to the spin-splitting effect. From a structural chemistry perspective, the magnitude of the spin-splitting effect crucially depends on the noncovalent and electrostatic interaction within the chiral perovskite, which induces the local site and long-range bulk inversion symmetry breaking. In this regard, we systematically retrospect the structure−property relationships in chiral perovskite. Insight into the rational design of chiral perovskites based on molecular configuration, dimensionality, and chemical composition along with their effects on spin-splitting manifestation is presented. Lastly, challenges in purposeful material design and further integration into chiral perovskite-based spintronic devices are outlined. With an understanding of fundamental chemistry and physics, we believe that this Perspective will propel the application of multifunctional spintronic devices.

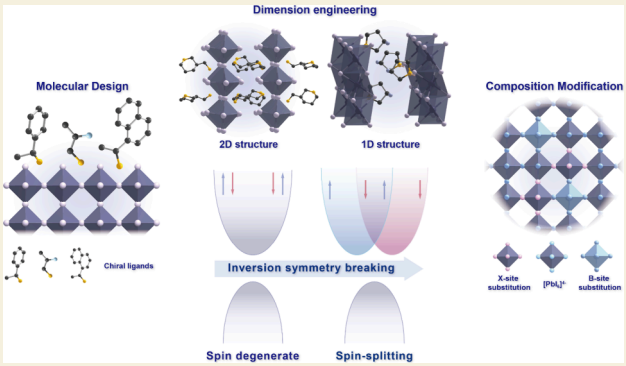

KEYWORDS: *Spin splitting, Chirality transfer, Spin−orbit coupling, Inversion symmetry breaking, Asymmetric hydrogen bonds, Lattice distortion*

1. INTRODUCTION

Hybrid organic−inorganic perovskite has demonstrated intriguing optical and electrical properties, which prompted extensive development of such a material family within the realm of multiple optoelectronics including photovoltaics, light emitting diodes, and photodetectors.[1−5] Following the progress in perovskite-based optoelectronic devices, the exploration and evolution of chiral perovskite with various chirality transfer mechanisms from organic components to inorganic lattice also quickened research interest of these compounds in the field of spintronics applications.[6,7]

Chiral perovskites combine chiral organic and achiral inorganic building blocks to facilitate a material system with promising chiroptical properties, which is attributed to the chirality transfer from the chiral ligand to the inorganic lattice. The abundant compositional and structural versatility of chiral perovskites engenders tunable chiroptical absorption and emission wavelength, long charge carrier lifetime, low trap densities, and novel spin-dependent properties. These unique characteristics empower chiral perovskite-based spintronic devices have to control over light, spin, and charges, thereby compensating for the inferior charge transport and optical response observed in organic chiral materials.[8−10] Notably, the intrinsic large spin−orbit coupling (SOC) and tunable Rashba-Dresselhaus effect of chiral perovskite offer electron spin manipulation as a new degree of freedom, which expands the functionalities of conventional electronic devices by coupling the electron's momentum with spin states.[11,12]

The extension of chirality in the perovskite lattice via abundant chemical bonding interactions would transfer the molecular stereochemistry across length scales and govern the spatial inversion symmetry breaking in the inorganic lattice. In this regard, chiral perovskite provides a promising material platform to study and harness the spin-splitting effect.[13−16] Based on the broad choice of organic and inorganic components, both crystal structures and the spin-splitting effect have been studied in some practical examples of chiral perovskite. However, the early studies have not been systematically reviewed to conclude the structure−property relationship that elucidates the translation of structural chirality to band-splitting.

Received: December 27, 2023
Revised: February 28, 2024
Accepted: March 7, 2024
Published: March 21, 2024

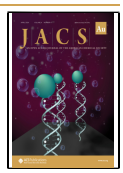

https://doi.org/10.1021/jacsau.3c00835
JACS Au 2024, 4, 1263−1277

Scheme 1. Chemical Strategies on Enhanced Spin-Splitting in Chiral Perovskite

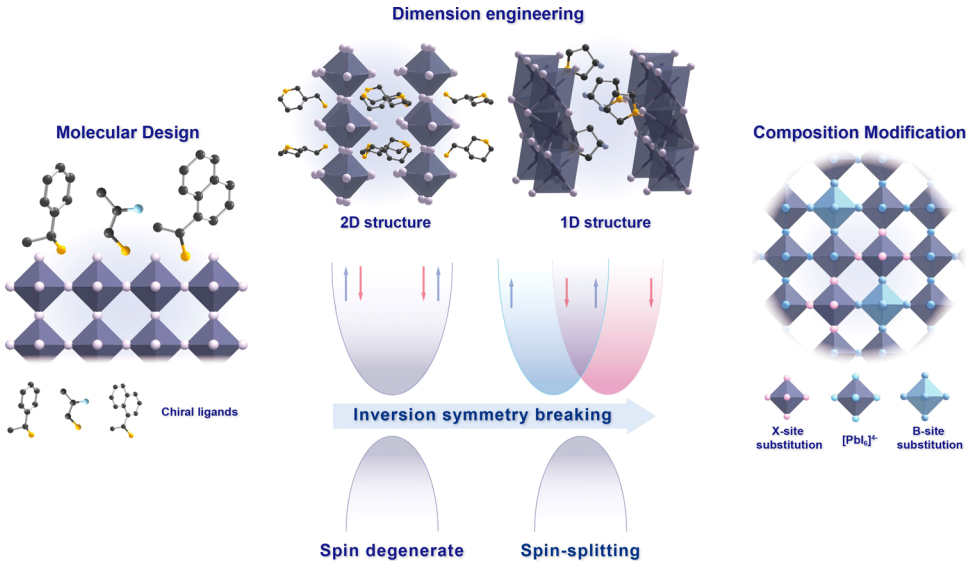

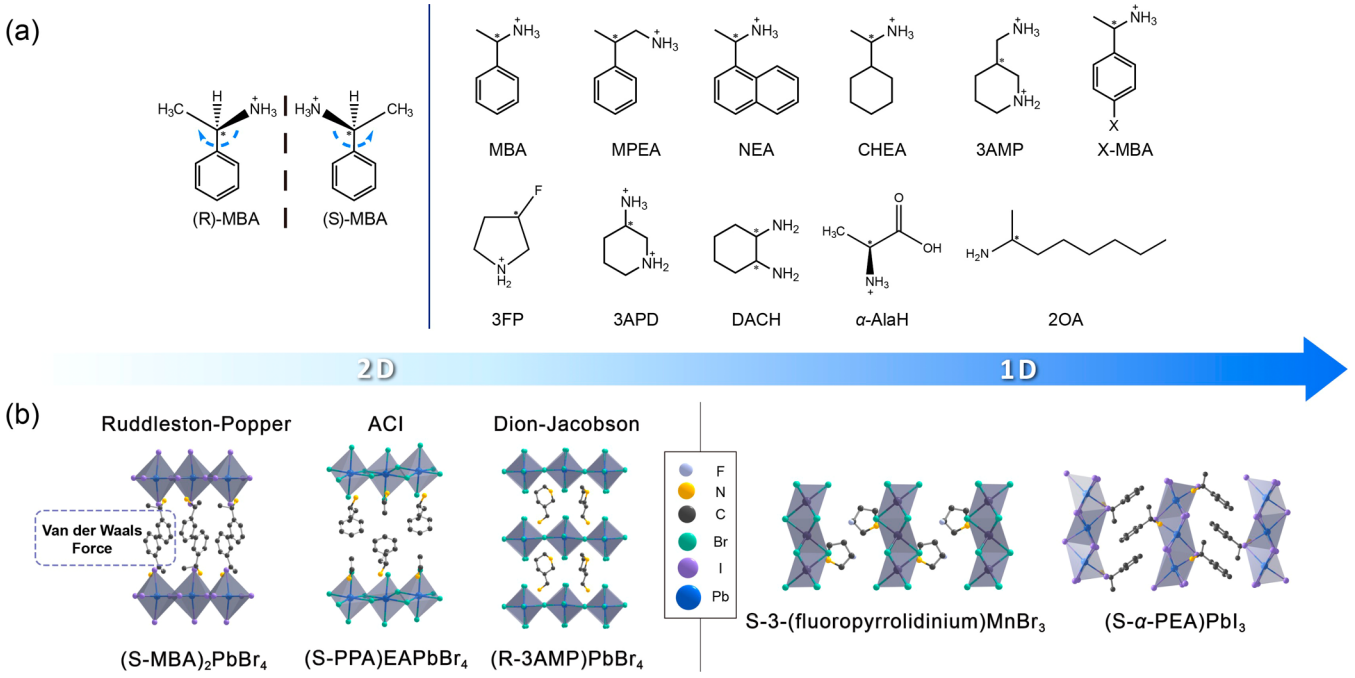

Figure 1. Representative chiral organic cations and chiral perovskite. (a) Representative chiral organic cations involved in the formation of chiral perovskite: MBA^+ (methylbenzylammonium),[18] $MPEA^+$ (β-methylphenethylammonium),[19] NEA^+ (1-(1-naphthyl)ethylammonium),[15] $CHEA^+$ (1-cyclohexylethylammonium),[20] $3AMP^{2+}$(3-(aminomethyl)-piperidine divalent cation),[21] X-MBA^+(4-fluoro- or chloro- or bromo- or nitro-methylbenzylammonium),[22,23] $3FP^+$ (3-fluoropyrrolidinium),[24] $3APD^{2+}$ (3-aminopiperidinium),[25] DACH (1,2-diaminocyclohexane),[26] α-Alah (protonated α-alanine),[27] 2OA (2-octylamine).[28] (b) Crystal structures of some typical chiral perovskites.

Besides, the lack of targeted structural design strategies hindered the rational control and optimization of chiral perovskite.

In this Perspective, we are committed to decoding the structural feature of chiral perovskite for achieving an enhanced spin-splitting effect. We focus on the material basis of chiral perovskites and how this specific material can be qualified for hosting considerable Rashba−Dresselhaus spin-splitting. Based on crystal structure analysis, we systematically retrospect the three structural design strategies that provide guidance for functionalized spin-splitting chiral perovskite, including molecular configuration, dimensionality, and chemical composition engineering, as depicted in Scheme 1. Our work suggests that the synergistic effect of multiple chemical bonding contributes to the asymmetric lattice distortion and is reflected in the electronic structure. Finally, a progressive outlook and challenges are presented for the advancement of chiral perovskites with diverse spintronic applications.

2. FUNDAMENTALS FOR CHIRAL PEROVSKITE SPINTRONICS

The effective spin transport and manipulation of chiral perovskites are prerequisites in a generic spintronic device. In terms of materials development, a hybrid organic−inorganic perovskite with a large spin−orbit coupling effect and related

https://doi.org/10.1021/jacsau.3c00835
JACS Au 2024, 4, 1263−1277

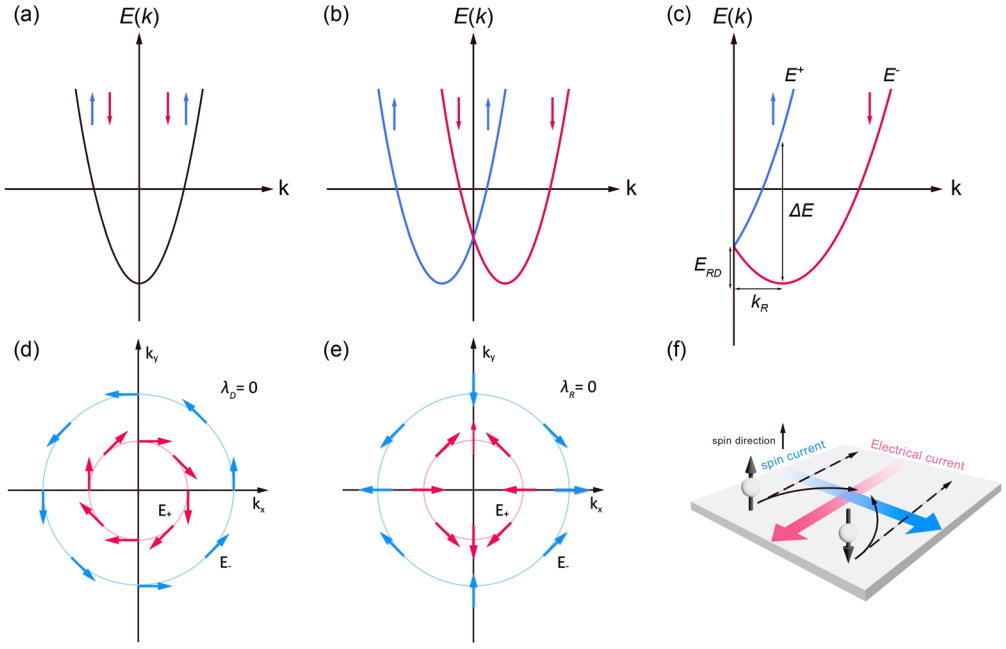

Figure 2. Rashba and Dresselhaus spin-splitting in a chiral perovskite. Schematic illustration of (a) a spin-degenerate electronic band. (b) Band dispersion including spin-splitting effect due to the SOC and inversion symmetry breaking. (c) Energy difference (ΔE) and momentum splitting (k_R) between inner (E_+, in red) and outer (E_-, in blue) sub-bands. Reproduced with permission under a Creative Commons CC-BY 4.0 license from ref 15. Copyright 2020 The Authors, published by Springer Nature. Schemes of spin textures for (d) pure Rashba and (e) pure Dresselhaus spin-splitting. Reproduced from ref 12. Copyright 2015 American Chemical Society. (f) Scheme of the Spin Hall effect.

Rashba–Dresselhaus effect is considered a pioneering candidate for the next generation of spintronics.[17] In this section, we first discuss the intrinsic characteristics of perovskites for their implementation in spintronics and the origin of the Rashba-Dresselhaus effect. Based on these understandings, we try to reveal structure–property relationships, which would offer guidance for designating perovskites with structural peculiarities for enhanced spin-splitting.

2.1. Material Basis of Chiral Perovskite

The archetypical perovskite with the chemical formula ABX_3 usually consists of $[BX_6]^{4-}$ octahedra with monovalent ammonium cations embedded in the cavities to neutralize the charges.[29] The presence of heavy elements in the crystal structure induces a strong SOC effect, which would give rise to the Rashba–Dresselhaus effect in noncentrosymmetric systems. With the integration of chiroptical properties, photoinduced spin-charge interconversion in chiral perovskite with spin-splitting could provide a route to optically addressable spintronics without the use of external magnetic fields.[12,30] Moreover, the fundamental bandgap may become indirect and influence the dynamics of charge carriers, which potentially leads to suppressed recombination and a longer charge carrier lifetime.

Not only the novel electronic structure complication but also perovskites with both abundant composition and corresponding crystallographic configurations underlie its advantageous physicochemical and optoelectronic properties. Within bulk perovskite, the existence of the spin-splitting effect was corroborated theoretically and experimentally.[12,14,31] The observation of those dynamic or static Rashba effects arising from structural fluctuations and lattice symmetry alterations remains a subject under exploration but is still limited.

Through chemically accomplished dimensionality reduction, the large templating organic ligands disrupt the Goldschmidt tolerance criterion and slice the bulk perovskite along different (hkl) planes or even confine the perovskite lattice within the nanoscale in three directions. These low-dimensional structures feature a combination of chiral ligands and inorganic sublattices for enhancing the transfer of chirality.[32] As shown in Figure 1, typical chiral organic cations and perovskite structures are represented. On one hand, the steric hindrance and bulkiness of the ligands will lead to different connection modes inside the inorganic sublattice including corner-sharing, edge-sharing, and face-sharing.[33] Specifically, the amount and rigidness of substituent groups on or near the protonated ammonium site will impose different degrees of strain on the inorganic sheets. On the other hand, the noncovalent intermolecular interactions inside the organic layer will rearrange the spatial conformation and packing characteristics of ligands. The different patterns inside the alternating organic and inorganic layers will therefore provide enriched tactics to promote symmetry breaking.[34]

2.2. Spin-Splitting Effect

In crystal materials, electronic wave functions are modulated by the periodic lattice potential, which is manifested as an electric field denoted as the gradient of crystal potential $E = -\nabla V(r)$. In the reference frame of electrons, the interaction between the momentum of electrons and crystal field will generate an effective magnetic field defined as follows:[30,35]

$$B_{\text{eff}} = \frac{\hbar}{2m^2c^2g\mu_B}[\nabla V(r) \times p] \quad (1)$$

This magnetic field induces a relativistic effect called the spin–orbit coupling effect. In the absence of either time-reversal symmetry or spatial inversion symmetry, the spin-degenerate spin up and spin down states $\varepsilon^{\uparrow}_k$ and $\varepsilon^{\downarrow}_k$ in k-space are lifted by SOC.[36,37] The valence band maxima and/or conduction band minima are shifted away from the symmetry points in the Brillouin zone, which give rise to the Rashba or Dresselhaus

https://doi.org/10.1021/jacsau.3c00835
JACS Au 2024, 4, 1263–1277

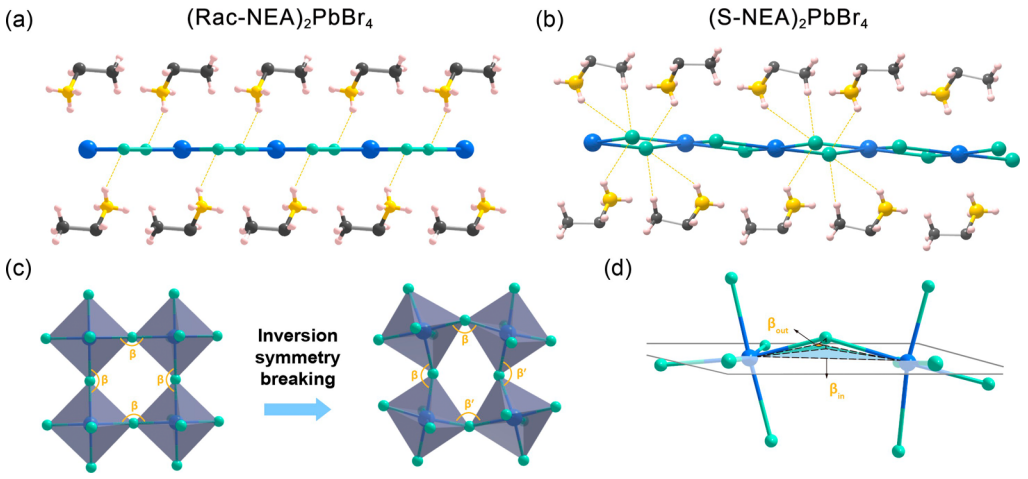

Figure 3. Asymmetric hydrogen bonds and structural symmetry breaking in a chiral perovskite. Hydrogen bonds between equatorial Br atoms and NEA cations in (a) $(Rac\text{-}NEA)_2PbBr_4$ and (b) $(S\text{-}NEA)_2PbBr_4$. (c) Symmetry breaking and its manifestation in Pb−X−Pb bond angle disparity, $\Delta\beta = \beta' - \beta$. (d) In-plane and out-of-plane asymmetric tilting of the octahedron. Reproduced with permission under a Creative Commons CC-BY 4.0 license from ref 22. Copyright 2021 The Authors, published by Springer Nature.

effects, as illustrated in Figure 2a,b.[12] The magnitude of the spin-splitting effect can be evaluated both qualitatively and quantitively. Since the energy band get shifted along the reciprocal lattice k in the presence of spin-splitting effect, the magnitude of spin-splitting effect can be studied quantitively with splitting factors, $\alpha = \Delta E/2k_R$.[38] The splitting factor is calculated by the eigenvalue difference versus the band edge shift along the k space (Figure 2c). The occurrence of Rashba or Dresselhaus coupling is linked to either local or extended inversion symmetry breaking. Specifically, Rashba coupling is induced by the structural inversion symmetry breaking while Dresselhaus effect is attributed to the macroscopic inversion asymmetry, usually arising from crystal space group of bulk materials.[34,39] Both effects feature characteristic spin textures and would coexist in one system (Figure 2d,e). The absence of magnetic properties in chiral perovskites arises from the preservation of time-reversal symmetry within the electronic structures. Therefore, the Rashba-Dresselhaus spin-splitting effect only emerges in perovskite materials that lack spatial inversion symmetry.[35,40] Once the inversion asymmetry is induced, the spin-splitting effect will enable the conversion of unpolarized charge current into net spin current and underlies the application of many spintronic device concepts, which is known as spin Hall effect, as shown in Figure 2f.[41−43]

2.3. Structure−Property Relationships

A comprehensive exploration of the Rashba−Dresselhaus spin-splitting effect in chiral perovskites necessitates a detailed investigation into structure−property relationships.[44] The lattice softness of chiral perovskites provides the solid foundation for efficient chirality transfer through the chiral ligand-induced chemical bonding environment. From a chemical perspective, the interplay among ionic, covalent, and noncovalent bonds within the perovskite framework instigates inherent symmetry breaking and influences the magnitude of spin-splitting. The phenomenon of chirality transfer can be triggered through four distinct mechanisms: (1) chiral distortion of the surface lattice; (2) chiral ligand mediated crystallization into chiral structures; (3) chiral patterning of surface ligands; (4) electronic interactions between organic and inorganic sublattices.[45−48]

In chiral perovskites, the presence of chiral ligands and their respective mechanisms (1) and (2) are widely observed. Mechanism (1) is caused by the interaction between chiral ligands and the surface of core materials (e.g., quantum dots and nanoplatelets), and mechanism (2) happens in chiral crystal-structured perovskite requiring a Sohncke space group to describe the global structure. Chiral perovskite belongs to 65 Sohncke space groups within 11 chiral point groups, encompassing 1 (C_1), 2 (C_2), 222 (D_2), 4 (C_4), 422 (D_4), 3 (C_3), 32 (D_3), 6 (C_6), 622 (D_6), 23 (T), and 432 (O). Among these, five are polar (C_1, C_2, C_3, C_4, and C_6) and enable ferroelectricity according to Neumann−Curie principles.[6,49] Therefore, from a crystallography perspective, we intuitively expect that chiral perovskites are potential Rashba materials due to the inversion symmetry breaking coupled with the SOC effect. However, it is acknowledged that the incorporation of chiral ligands often templates low-dimensional structures, complicating the transformation mechanism of crystal symmetry into the manifestation of spin-splitting. Merely focusing on global crystal symmetries may prove to be insufficient for predicting the strength of band splitting. This is because the noncentrosymmetric global space groups primarily stem from the organic ligands, while the inorganic components contribute to the SOC effect. In some cases, the constituent inorganic layers almost retain the inversion symmetry despite adopting global Sohncke space groups with the whole structure, which underlies limitations in the manifestation of strong spin-splitting.[22] With this fact in mind, understanding the crystal symmetry from its individual components to the whole structure would allow a more reliable search algorithm for identifying spin-splitting chiral perovskite.[13]

The localized structural features are reported to be scrutinized by the interoctahedral and intraoctahedral distortion parameters of $[BX_6]^{4-}$ in several instructive works.[50,51] The bond angle variance σ^2, bond length distortion Δd, and bond disparity between adjacent octahedrons $\Delta\beta$ are employed for a semiquantitative analysis of the local symmetry breaking:

$$\sigma^2 = \frac{1}{11}\sum_{\{i=1\}}^{12}(\alpha_i - 90)^2 \quad (2)$$

https://doi.org/10.1021/jacsau.3c00835
JACS Au 2024, 4, 1263−1277

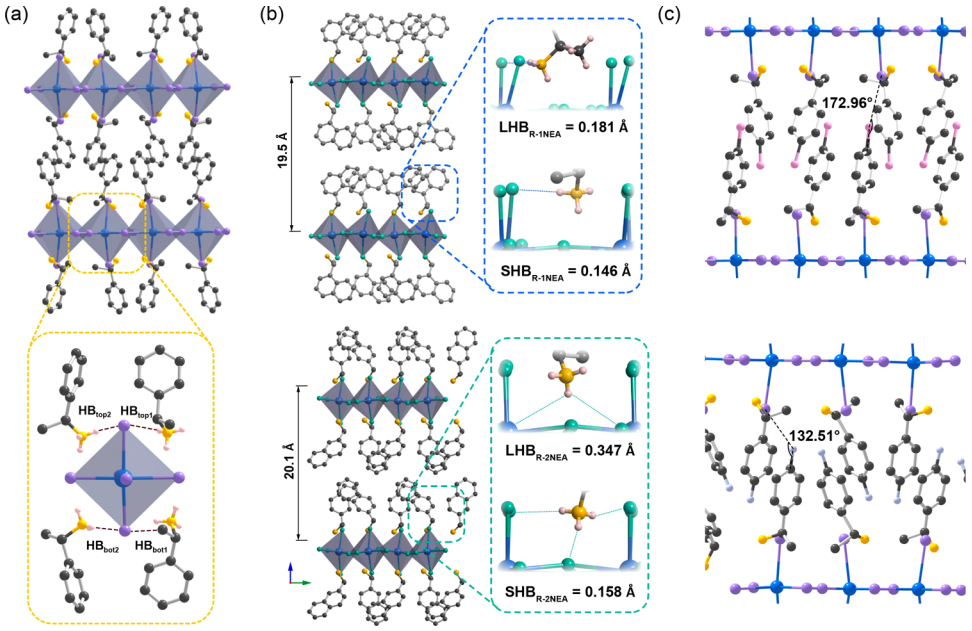

Figure 4. Asymmetric bonding environment induced by various chiral ligands. (a) Schematic illustration of the hydrogen bonds and distortion in the DFT-optimized structure of $MBA_2PbI_xBr_{4-x}$. Reproduced with permission under a Creative Commons CC-BY 4.0 license from ref 18. Copyright 2022 The Authors, published by Springer Nature. (b) Asymmetric NH_3^+ penetration depth and hydrogen bonds in $(R\text{-}1NEA)_2PbBr_4$ and $(R\text{-}2NEA)_2PbBr_4$. Reproduced with permission under a Creative Commons CC-BY 4.0 license from ref 59. Copyright 2023 The Authors, published by Springer Nature. (c) Different halogen-halogen interactions in $(ClMBA)_2PbI_4$ and $(FMBA)_2PbI_4$. Reproduced with permission from ref 23. Copyright 2021 John Wiley and Sons.

$$\Delta d = \frac{1}{6}\sum_{\{i=1\}}^{6}\left(\frac{d_i}{d_0}\right)^2 \tag{3}$$

$$\Delta\beta = \beta' - \beta \tag{4}$$

Here, α_i denotes the individual cis X−Pb−X bond angle; d_i is the B−X bond length, and d_0 corresponds to the mean B−X bond length; β' and β denote the asymmetric tilted B−X−B bonds, as shown in Figure 3c. In an ideal octahedron maintaining inversion symmetry, we can infer a zero σ^2, $\Delta\beta$ with $\Delta d = 1$. Oppositely, the loss of inversion symmetry will indicate a large variation in bond length and angle, reflecting in a nonzero σ^2 or $\Delta\beta$, concomitant with a Δd deviated from 1. By these descriptors, a more detailed inversion symmetry breaking picture can be elaborated.

To gain insight into the local symmetry of the inorganic sublattice, refined structural studies are needed to identify the bonding interactions and their correlation with the localized structural features. In low-dimensional chiral perovskite, the terminal ammonium group ionically interacts with and hydrogen bonds to the extended $[PbX_6]^{4-}$ octahedrons, with the tail groups sterically interfering with the inorganic sheets.[51] The microscopic asymmetric hydrogen bonds-dominated distortion and band-splitting have been exemplified by Mitzi's group.[15,22,52] They reported a puckered square arrangement of the adjacent four octahedra templated by the asymmetric hydrogen-bonding in $(R/S\text{-}NEA)_2PbBr_4$ (NEA = 1-(1-naphthyl)ethylammonium). Within an inorganic layer, on one side, two equatorial Br atoms H-bond with both NH_3^+ and α-CH_3 groups in NEA^+; while on the opposite side, only one hydrogen bond with NH_3^+ is found (Figure 3a,b). The asymmetric hydrogen bonds induce out-of-plane distortions, and the conduction band (CB) splits into two branches along the Γ−Z path with ΔE values up to 1.52 eV. The discontinuity of the inorganic lattice cut by the chiral ligand is in accordance with the lack of band dispersion along the Γ−X path, perpendicular to the inorganic lattice. Consequently, we conclude that the introduction of distortion or structural asymmetry in the inorganic sublattice by enriching and strengthening asymmetric noncovalent bonds would be the core objective to manipulate band-splitting. Besides, the bond disparity $\Delta\beta$, which positively correlates to the band splitting, could indicate the potential strength of spin-splitting from a structural viewpoint.

3. CHEMICAL STRATEGIES FOR ENHANCED SPIN-SPLITTING

3.1. Molecular Configuration Design

In chiral perovskite, the chiral ligand endows specific structural symmetry breaking onto the inorganic frameworks and encodes the asymmetry into their electronic states.[53] Hence, the molecular configuration of these chiral ligands plays a crucial role in creating an asymmetric chemical environment that extends across various levels. A chiral ligand comprises three components: a headgroup (a protonated ammonium), a chiral center, and tail groups. The headgroup, commonly a protonated primary ammonium, functioned to ionically interact with the octahedra; the bulky tail groups, which consist of aliphatic chains or conjugated rings, varying in steric hindrance mainly affect the strength of the asymmetric hydrogen bonds; and the chiral center guarantees both the chirality transfer and inversion symmetry breaking upon the inorganic lattice. Functionalizing a single ligand or introducing foreign ligands into the chiral perovskite system impacts the packing arrangement of ligands, introduces diverse noncovalent interactions, and governs the symmetry breaking in the inorganic sublattice. This section delves into these reported ligands and outlines a preliminary criterion for molecular configuration design.

https://doi.org/10.1021/jacsau.3c00835
JACS Au 2024, 4, 1263−1277

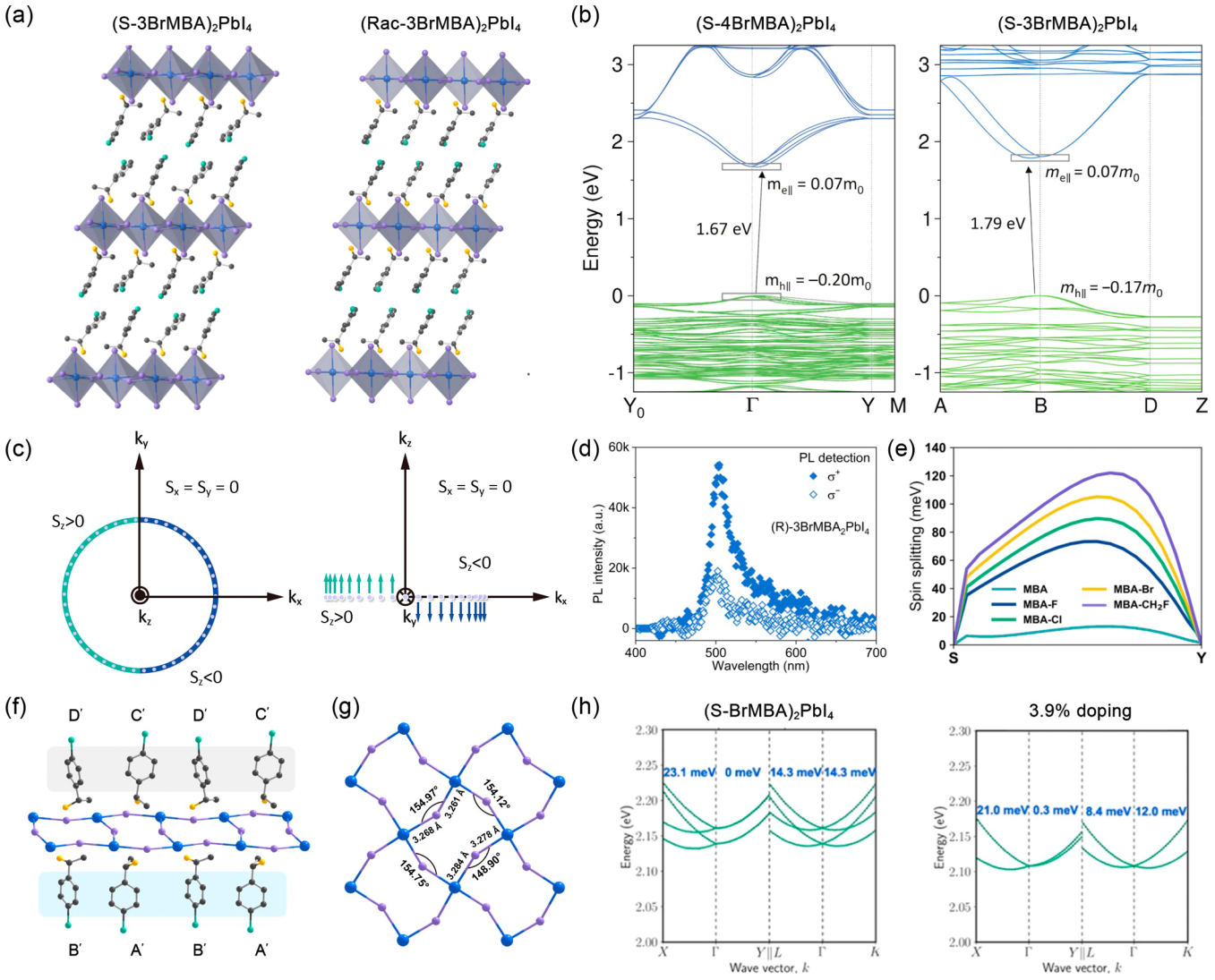

Figure 5. Ligand functionalization and doping strategies to amplify the spin-splitting effect. (a) Structure of (Rac/S-3BrMBA)$_2$PbI$_4$. (b) DFT calculated band structures of (S-3/4BrMBA)$_2$PbI$_4$. (c) Corresponding spin textures computed for the inner band. (d) Circularly polarized PL (CPL) spectra of the (*R*-3BrMBA)$_2$PbI$_4$ single crystals at room temperature. Reproduced with permission under a Creative Commons CC-BY 4.0 license from ref 61. Copyright 2023 The Authors, published by AAAS. (e) Spin-splitting energy along the S−Y direction in the corresponding chiral perovskite. Reprinted with permission from ref 62. Copyright 2021 American Chemical Society. (f) Arrangement and orientation of chiral ligands relative to the inorganic layers. (g) In-plane bond angle disparity illustration. (h) DFT calculation results of spin-splitting in the band structures along different k-paths for (S-BrMBA)$_2$PbI$_4$ and 3.9% doping ratio. Reprinted with permission from ref 65. Copyright 2023 American Chemical Society.

First, by considering the tail group of the chiral ligand, the structural diversity of the tail group induces various intermolecular interactions, ultimately governing the lattice distortion of octahedron frameworks. A notable trend is observed in conjugated ligand-based systems, and the presence of various aromatic bodies based on benzene, naphthalene, and other heteroarenes contributes to the existence of a large π bond (Π_6^6) with delocalized electrons. The intermolecular $\pi-\pi$ interactions arising from aromatic rings align the orientation of ligands and benefit the asymmetric distortion of the inorganic lattice.[54,55] Additionally, the $p-\pi$ coupling between the aromatic ligands and halide has been noted to modify the electronic structure of the 2D perovskite.[56] Ma et al. verified the intermolecular interactions of aromatic MBA (methylbenzylammonium) through the nanoconfined growth of chiral $MBA_2PbI_xBr_{4-x}$ (Figure 4a). A precise structural analysis of the strained lattice demonstrated that the stacking conformation of the MBA^+ varied depending on the lowest energy optimization of $\pi-\pi$ stacking under different confined constraints.[18] As shown in Figure 4a, the distinct intermolecular distance and angles between ligands induce four distinct hydrogen bonds and adjust the asymmetric hydrogen bonding environment. As a result, different conformational stacking of ligands under micro-strain amplifies the chiral distortion of the inorganic framework.

The chiral center location and the degree of steric hindrance also significantly influence lattice distortion and chirality transfer. In chiral perovskites, when the chirality center is situated at the α-position, stronger chirality is observed compared to when it is on β-position;[57,58] Effective inversion symmetry breaking is also attributed to the steric hindrance effect of the chirality center, where the location and bulkiness of the functional group directly modify the penetration depth and the strength of the hydrogen bonds. To investigate the steric hindrance effect, Son et al. chose two structural isomers-based (R/S-1NEA)$_2$PbBr$_4$ and (R/S-2NEA)$_2$PbBr$_4$ (NEA = naph-

https://doi.org/10.1021/jacsau.3c00835
JACS Au 2024, 4, 1263−1277

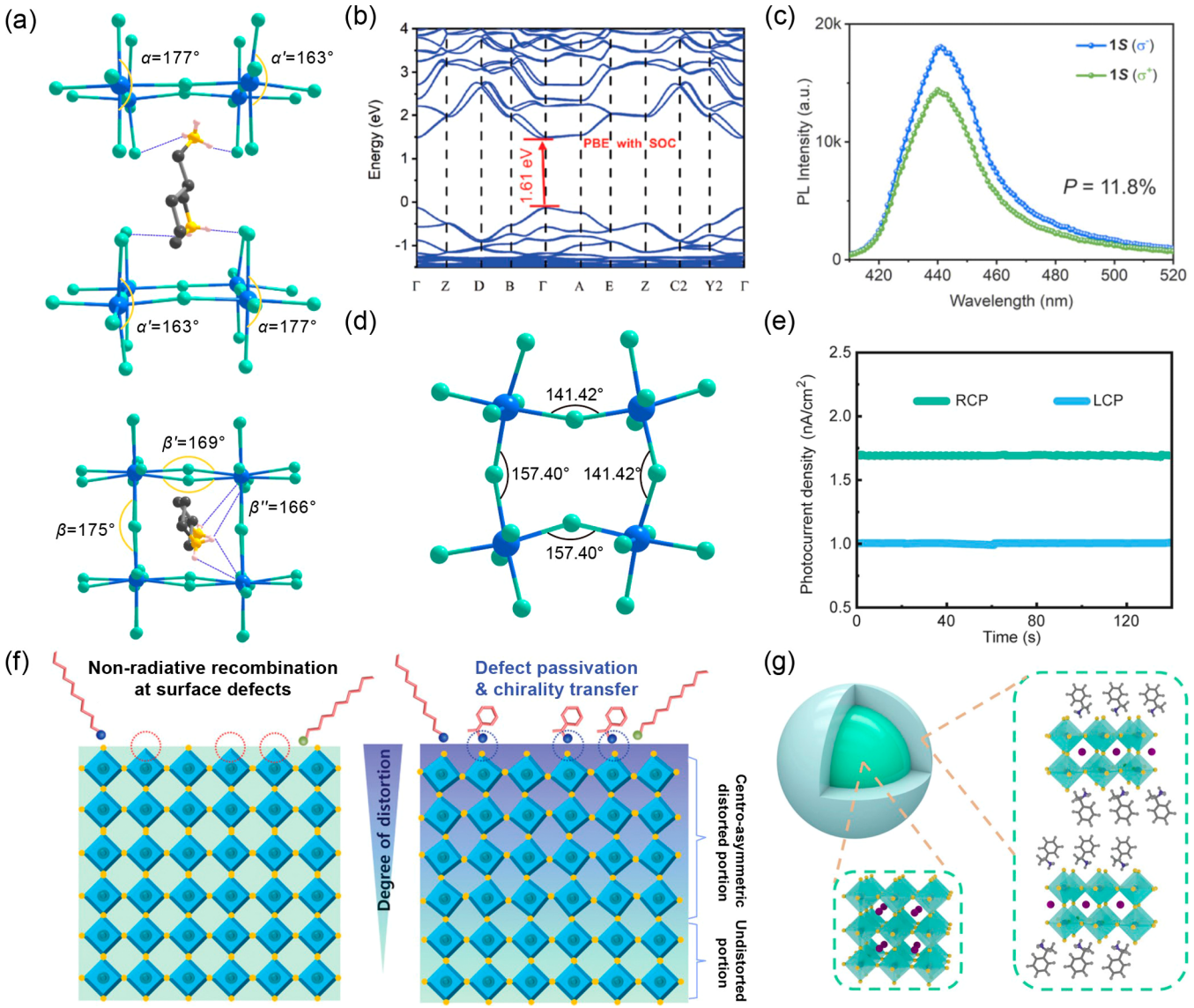

Figure 6. Dimension engineering in chiral perovskite. (a) In-plane and out-of-plane bond angle disparity of the inorganic sublattice in (R-3AMP)$PbBr_3$. (b) DFT calculated band structures and projected density of states of (*R*-3AMP)$PbBr_3$. (c) Circular polarized light excited photoluminescence spectra of (*S*-3AMP)$PbBr_4$ Reproduced with permission from ref 21. Copyright 2022 John Wiley and Sons. (d) Equatorial bond angle disparity of Pb−Br−Pb in (*R*-PPA)$EAPbBr_4$. (e) Photocurrent density dependent time under LCP, RCP light illumination at 0 V bias of (*R*-PPA)$EAPbBr_4$. Reprinted from ref 71. Copyright 2022 American Chemical Society. (f) Schematic illustration of chirality transfer in perovskite nanocrystals with chiral ligand decorated on the surface. Reproduced with permission under a Creative Commons CC-BY 4.0 license from ref 73. Copyright 2022 The Authors, published by John Wiley and Sons. (g) Scheme of the core−shell chiral perovskite nanocrystal. Reprinted from ref 74. Copyright 2022 American Chemical Society.

thylethylamine) according to the position of ethylamine on the naphthyl skeleton.[59] The naphthyl facilitates a different blocking effect on the penetration of amine groups, consequently promoting distortion of the inorganic frameworks. Specifically, the conformational changes of the naphthyl isomers in both recumbent and vertical orientations invoke differences in both the amount and strength of hydrogen bonds. As shown in Figure 4b, $(R\text{-}2NEA)_2PbBr_4$ exhibits a more severe octahedral distortion, with an asymmetric bond angle disparity ($\Delta\beta$) up to 14.5°, which could lead to a substantial spin-splitting effect.

Furthermore, the modification of asymmetric hydrogen environment through the functionalization of chiral ligands and ligand doping strategy also holds significance in inducing symmetry breaking.[60] Lin et al. synthesized $(4\text{-}XMBA)_2PbI_4$ compounds (X = H, F, Cl, Br) by intentionally halogenating the para-site of the phenyl rings. By studying the single crystal structure of $(FMBA)_2PbI_4$ and $(ClMBA)_2PbI_4$ in Figure 4c, a halogen bond between the para-halogen atom and the axial iodine of the octahedron is found to be significantly different.[23] The synergetic effect of halogen−halogen bond interactions and *d*-spacing in $(ClMBA)_2PbI_4$ harnessed the largest distortion. To gain more detailed insight into the structure−property relationship, Liu et al. recently reported (R/S)-$3BrMBA_2PbI_4$ [3BrMBA = 1-(3-bromphenyl)-ethylamine], with the crystal structure depicted in Figure 5a.[61] (S)-$3BrMBA_2PbI_4$ exhibits a homogeneously distributed β with two distinct values, while (S)-$4BrMBA_2PbI_4$ is observed with a more disordered distribution of β, suggesting the larger microstrain. Compared to the para-site substituted Br-MBA, the metaposition of Br atoms in 3-BrMBA induced a larger polar distortion with $\Delta\beta$ = 11.9°,

https://doi.org/10.1021/jacsau.3c00835
JACS Au 2024, 4, 1263−1277

indicating a sizable Rashba effect and α up to 2.21 eV Å in the conduction band, which consists of lead 6*p* orbitals and a little iodine 5*p*, as shown in Figure 5b. The incomplete splitting is observed in only one direction (B−A) and results in a special spin texture (Figure 5c). The collected circularly polarized PL spectra in Figure 5d indicate a degree of polarization up to ∼0.52. Besides, it has also been reported by Wei and co-workers that the halogen substitution will lead to a distinct electrostatic potential surface of the chiral ligands.[62] This local electrical field induces distortion of the $[PbI_6]^{4-}$ octahedron. The calculated band structures in this work suggest the largest α up to 1.209 eV Å in (*S*-MBACH$_2$F)PbI$_3$ (MBACH$_2$F = 1-fluoro-2-phenylpropan-2-ammonium), which is depicted in Figure 5e.

Since chemical functionalization needs complicated techniques, ligand doping emerges as a pragmatic approach to annihilate the structural inversion symmetry elements via highly directional noncovalent interaction.[63] Yan et al. demonstrated this by introducing a mixed aryl-alkyl perovskite comprising chiral aryl cations (R/SMePEA = β-methylphenethylammonium) and achiral alkyl cations (C4A = butylammonium). The one-to-one matched (sp^3) CH$\cdots\pi$ interaction imposes a noncentrosymmetric $P2_1$ symmetry within the perovskite sheet, indicating the potential existence of spin-splitting.[19] Similarly, Lee et al. tailored the structure and charge transport properties of perovskite lattice through the incorporation of urea into S-MBA$_2$PbI$_4$.[64] The molecular rearrangement of the urea and MBA cations is unveiled by solid-state NMR and magic-angle spinning NMR spectra and realized an $\Delta\beta$ estimated up to 31.73°, one of the largest observed in chiral perovskites. Xie and colleagues reported a 3.9% doping amount of S-2-MeBA (2-MeBA = 2-methylbutylammonium) into (S-BrMBA)$_2$PbI$_4$ (BrMBA = 4-bromo-α-methylbenzylammonium), which enables the distinct structural change and lifts the restricted distortion of perovskite lattice. The doping strategy leads to a *P*1 symmetry of the inorganic lattice, which enjoys a $\Delta\beta$ of 6.07° (Figure 5f,g) and a spin-splitting of ΔE = 21 meV (Figure 5h).[65]

3.2. Dimension Engineering

Ligand versatility in chiral perovskites not only exerts local strain on the inorganic lattice but also templates the growth of inorganic lattice with different connectivity modes, forming 2D, 1D, 0D, and nanocrystal patterns. As the bulk lattice gradually contracts into the chained networks or even 0D clusters, an increase in chiral organic moieties ratio will greatly promote symmetry breaking but reduce the orbital overlap and sacrifice the charge transport to some degrees. In this section, we aim to convey an idea on dimension engineering to address the balance between symmetry breaking and semiconductor properties.

The chirality of organic cations is always accompanied by a branched structure. Therefore, most chiral perovskites are found to be 2D and quasi-2D configurations because the bulky chiral ligands can hardly fit into the cavity within the bulk perovskite lattice. Within the realm of 2D chiral perovskites, they are further categorized into Ruddlesden−Popper (RP) phases, and the Dion−Jacobson (DJ) phases, while the alternating-cation-interlayer (ACI) phase has been rarely reported due to the limitation of chiral ligands.[66] Studies have indicated that compared to RP phases, DJ phases exhibit a synergistic effect of polar and chiral structures. The polar structure inherently generates an electric field, enhancing spin-splitting effects.[67,68] The in-plane polarization in chiral polar perovskite could manipulate the spin direction of each sub-band by the electrical reverse of polarization direction along the polar axis. Moreover, the diammonium spacers bridged the adjacent inorganic layers with electrostatic interactions, thus, eliminating the van der Waals gaps. A more closely packed structure will induce both in-plane and axial spin-splitting effect. Notably, recent observations in (R/S-3AMP)PbBr$_4$ (3AMP = 3-(aminomethyl)-piperidine divalent cation) have revealed substantial spin-splitting effects within this DJ phase.[21] The novel chiral ligand templated a chiral and polar structure, which occurs with an out-of-plane angle disparity $\Delta\alpha$ = 14° and an in-plane $\Delta\beta$ = 9°, as shown in Figure 6a. The splitting factor in this DJ phase is calculated up to 0.93 eV Å in the conduction band minimum (Figure 6b). This Dion−Jacobson chiral perovskite Rashba ferroelectric displays high CPL sensitivity, which indicates a large spin-splitting effect in the chiral polar structure (Figure 6c).

In 2D phases, the layer-dependent band-splitting in chiral perovskite also plays an integral role while it is scarcely discussed. In n = 1 perovskite, the out-of-plane tilt is usually negligible (with $\Delta\beta_{out}$ being very small), and only in-plane distortion is taken into consideration. In the presence of the small A-site cations in quasi-2D perovskite (n > 1), the small cations will play a vital role in the local symmetry breaking like the bulk perovskite. The steric effects from the A-site cations will induce out-of-plane distortion, possibly due to the accumulating internal charge and structural mismatch with the addition of small cations inside the inorganic layers.[69] It is worth mentioning that some works have also demonstrated that with the further increase of inorganic layer ($n \geq 2$), the distortion decreases, same as the band-splitting.

Beyond 2D structures, the 1D phase also emerges in chiral perovskites to accommodate the large spatial steric effect of chiral ligands. In 1D chiral perovskite, edge-sharing and face-sharing connectivity modes feature pronounced distortion in bond length and angle, contributing to enhanced symmetry breaking. For instance, chiral α-phenylethylamine (α-PEA) a has been reported as a templating cation in the 1D chiral perovskite, demonstrating a distorted orthorhombic crystal system.[70] A chiral ferroelectric 1D perovskite, (R/S-CYHEA)PbI$_3$ (CYHEA = cyclohexylethylamine) has been proven to form an indirect bandgap with a strong spin-splitting effect.[20] Owing to the largest fraction of chiral ligands in 1D perovskite, greater octahedral bond-length distortion, and potentially large chiroptical response are reported compared with 2D structures.[70] However, the unidirectional extension of the octahedra in the 1D phase exacerbates the recombination of charge carriers. Zhu et al. discussed the trade-off between lattice distortion and charge transport in 2D and 1D structures.[71] By incorporating short-chain ligand EA (EA = ethylammonium) into the precursor containing the reactants for 1D (R/S-PPA)PbBr$_3$ (PPA = 1-phenylpropylamine), they obtained an ACI type perovskite (*R*/*S*-PPA)EAPbBr$_4$. The packing structure of this chiral perovskite verifies an acentric $P2_1$ space group with $\Delta\beta$ up to 16°, which enriches the chemical methods to promote asymmetric lattice distortion (Figure 6d). Steady photocurrent densities under right-handed circularly polarized (RCP) and left-handed circularly polarized light (LCP) in Figure 6e with g_{res} of about 0.42 suggest a stable distinguishing ability.

It has also been found that the post-attachment of chiral ligands onto the nanocrystal surface could engender chirality transfer, which provides an ideal material platform for structural tunability.[72] The complicated surface chemistry of chiral perovskite nanocrystals leads to a more intricate chirality transfer mechanism, including both electronic coupling and asymmetric lattice distortions.[26] As shown in Figure 6f, a

https://doi.org/10.1021/jacsau.3c00835
JACS Au 2024, 4, 1263−1277

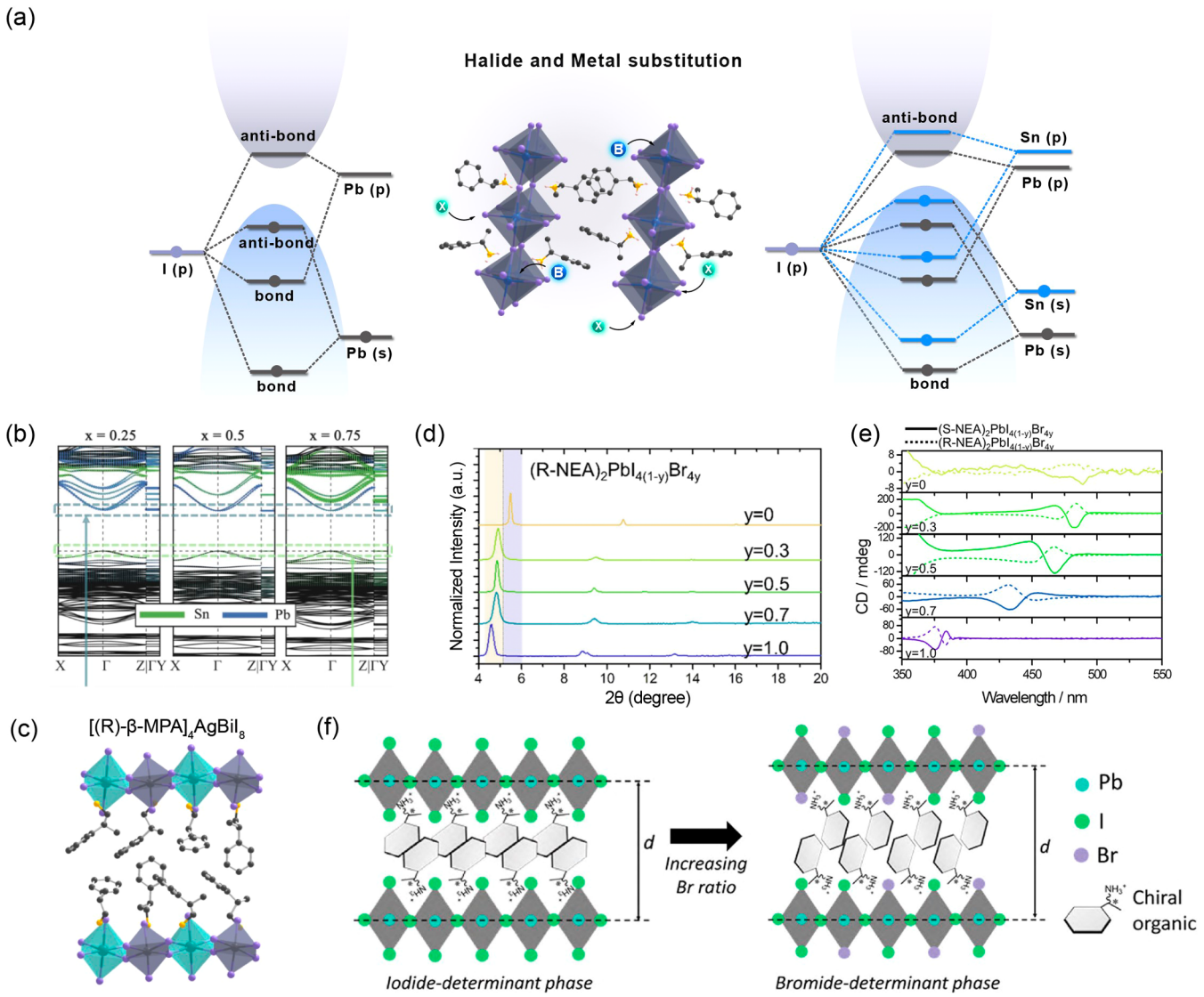

Figure 7. Chemical composition modification for effective symmetry breaking. (a) Schematic illustration of electronic structure change and lattice distortion in chiral perovskite through metal substitution. (b) Computed DFT+SOC electronic band structures of $(S\text{-}MBA)_2Pb_{1-x}Sn_xI_4$ derived from Pb and Sn. Reprinted from ref 54. Copyright 2020 American Chemical Society. (c) Crystal structure of $[(R)\text{-}\beta\text{-}MPA]_4AgBiI_8$. Reproduced with permission from ref 76. Copyright 2021 John Wiley and Sons. (d) XRD patterns of $(S\text{-}NEA)_2PbI_{4(1-y)}Br_{4y}$ and $(R\text{-}NEA)_2PbI_{4(1-y)}Br_{4y}$ with gradually enlarged *d*-spacing with Br incorporation. (e) CD spectra of $(S\text{-}NEA)_2PbI_{4(1-y)}Br_{4y}$ and $(R\text{-}NEA)_2PbI_{4(1-y)}Br_{4y}$. (f) Schematic illustration of the I/Br replacement and phase transition. Reprinted from ref 81. Copyright 2020 American Chemical Society.

detailed crystallographic study of S-MBA$^+$ decorated $CsPbBr_3$ nanocrystals reveals that the surface chiral ligands induce a centro-asymmetric distortion that would theoretically penetrate fifth layer of the inorganic lattice.[73] In addition, a delicate chiral core−shell structure with an elaborate chemical technique is realized based on perovskite nanocrystals. By virtue of such a chiral-achiral structure with type II band alignment, both the chirality transfer and charge transport can be guaranteed (Figure 6g).[74] Theoretical calculations also confirmed a Rashba spin-splitting effect both in the CB minimum (CBM) and VB maximum (VBM).

3.3. Modification of Chemical Composition

The unique electronic band structure observed in chiral perovskites stems from the intricate hybridization of metal and halogen atom orbitals. For instance, considering the prototypical $MAPbI_3$, the valence band maximum is a hybridization of I 5*p* and Pb 6*s* orbitals, preserving the *s* symmetry; whereas the conduction band minimum originates from the spin−orbit spin-off states of the Pb 6*p* orbitals,[75] the chemical composition of inorganic lattice and the structure perturbation will directly impact the spin-splitting. Because the templating ligands hardly participate in the construction of the band edge states, in this section, we only discuss the compositions of the B/X site and the corresponding impact on the manifestation of the spin-splitting effect.

In the case of metal cation substitution, the Goldschmidt tolerance factor should be taken into consideration since different outer electronic structures of metal cations will determine not only the structural stability but also the dimensionality of the chiral perovskite. The valence state of metal cations in perovskites allows categorization into different types: divalent metal-based perovskite (involving Pb, Sn, Ge on the B-site); Trivalent metal-based perovskite (with Sb, Bi on the B-site); Tetravalent metal-based perovskite (with Mn on the B-site); and double perovskite (comprising dual metal cations such

https://doi.org/10.1021/jacsau.3c00835
JACS Au 2024, 4, 1263−1277

Table 1. Asymmetry Distortion, Splitting Factors, and Degree of Chirality of Chiral Perovskites

Molecular structure	Chemical formula	Space group	$\Delta\beta$ (°)	α (eV Å)	Chirality degree	Design strategy	Synthesis method
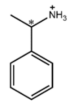	(S-MBA)$_2$PbI$_4$[35,88,89]	$P2_12_12_1$	5.9	0.75	CD ≈120 mdeg (510 nm) P = 1 × 10-1	Molecular design	Cooling crystallization
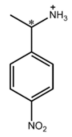	(S-4-NO$_2$-MBA)$_2$PbBr$_4$·H$_2$O[22]	$P2_1$	12.0	1.398	-	Molecular design	Cooling crystallization
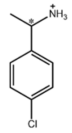	(R-4-Cl-MBA)$_2$PbBr$_4$[22,23]	$P2_12_12_1$	14.9	0.709	CD ≈ 100 mdeg (490 nm) g_{CD} = 3.1 × 10-3	Molecular design	Cooling crystallization
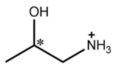	(S-HP1A)$_2$PbBr$_4$[44]	$P4_32_12$	13.3	-	CD ≈ -5 mdeg (400 nm) g_{CD} = -3 × 10-4	Molecular design	Antisolvent vapor-assisted crystallization
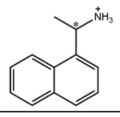	(S-NEA)$_2$PbBr$_4$[15]	$P2_1$	14.0	1.52	CD ≈ -20 mdeg (393 nm)	Molecular design	Cooling crystallization
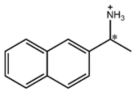	(R-2NEA)$_2$PbBr$_4$[59]	$P2_1$	14.5	-	CD ≈ -120 mdeg (382 nm) g_{CD} = -2.78 × 10-3	Molecular design	Antisolvent vapor-assisted crystallization
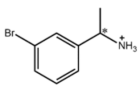	(R)-3BrMBA$_2$PbI$_4$[61]	$P2_1$	11.9	2.21	CD ≈ 30 mdeg (490 nm) P = 5.2 × 10-1	Molecular design	Cooling crystallization
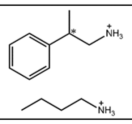	(S-MePEA)(C4A)PbBr$_4$[19]	$P2_1$	0.4	-	CD ≈-10 mdeg (400 nm) g_{CD} = -2.5 × 10-4	Molecular design	Slow evaporation
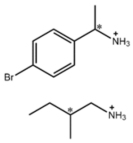	(S-BrMBA)$_x$(S-2MeBA)$_{1-x}$PbI$_4$ (3.9%) [65]	P1	6.1	-	CD ≈3 mdeg (508 nm) g_{CD} = 1.88 × 10-4	Molecular design	Slow evaporation
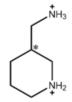	(R-3AMP)PbBr$_4$[21]	$P2_1$	9.0	0.93	CD ≈60 mdeg (425 nm) g_{CD} = 1.8 × 10-3 P = 1 × 10-1	Dimension engineering	Cooling crystallization
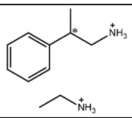	(S-PPA)EAPbBr$_4$[71]	$P2_1$	16.0	-	CD ≈ -30 mdeg (323 nm) g_{CD} = -2.5 × 10-3	Dimension engineering	Cooling crystallization
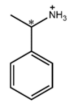	(R-MBA)$_2$SnI$_4$[54]	$P2_12_12_1$	0.3	-	CD ≈-5 mdeg (402 nm) P = 9.4 × 10-1	Composition modification	Cooling crystallization
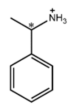	(S-β-MPA)$_4$AgBiI$_8$[76]	$P2_1$	-	-	CD ≈ -17 mdeg (515 nm)	Composition modification	Cooling crystallization

https://doi.org/10.1021/jacsau.3c00835
JACS Au 2024, 4, 1263−1277

as Ag, In in +1 and Sb, Bi in +3 states).[30] For example, Lu and colleagues detailed a Sn-based (*R*-/*S*-MBA)$_2$SnI$_4$ chiral perovskite exhibiting significant in-plane distortion of octahedra due to the closely interacted aromatic ligand via $\pi-\pi$ stacking.[21] The electronic band structure of Pb/Sn alloys is calculated to vary across different compositions, as shown in Figure 7a,b. Beyond the lead-based chiral perovskite, Li et al. developed lead-free double perovskites, [(R)-β-MPA]$_4$AgBiI$_8$ ((R)-β-MPA = (R)-(+)-β-methylphenethylammonium, **1-R**) and [(S)-β-MPA]$_4$AgBiI$_8$ ((S)-β-MPA = (*S*)-(−)-β-methylphenethylammonium, **1-S**). These compounds consist of an inorganic layer constructed by the alternating BiI$_6$ and AgI$_6$ octahedron, with the MPA cations distributed on the both sides (Figure 7c).[76] This result provided examples of efficient chiral transfer in lead-free chiral perovskites. Furthermore, perovskite chiral ferromagnets also stimulate research interest by incorporating Mn into the chiral perovskite system. As ferroelectric hybrid perovskites are inherently bulk inversion asymmetric, a significant Dresselhaus spin-splitting effect is anticipated.[24,77]

Apart from the chemical substitution on the B-site, the halide component also holds significant importance in the crystal structure and electronic structure of chiral perovskite. On one hand, the halide directly dominates the CBM and VBM of the chiral perovskite, which influences the carrier transport; in the other, the halogen atoms contribute to the local chemical bonding with the Pb atoms and thus the site symmetry and the extended bulk symmetry. In detail, the inversion symmetry breaking and band splitting in mixed-halide chiral perovskites are believed to originate from several mechanisms. First, the band splitting is rooted in the various halide bonding chemistries caused by different electronegativities of halogen atoms and enhanced by the symmetry breaking in certain doping ratios;[78] Second, the ion radius difference will promote the band splitting by a local residual strain, which will give rise to the lattice distortion in asymmetric systems;[79] Also, the inversion symmetry breaking is recently correlated with the ionic defect that produces a local electric field.[80] Since the defects can be directly engineered by alloying halide anions in chiral perovskites, the corresponding band structure and splitting will be modulated. Ahn et al. reported rapid crystalline structure changes and wavelength tunability of chiroptical phenomenon in (*S*/*R*-MBA)$_2$PbI$_{4(1-x)}$Br$_{4x}$ concerning different iodide/bromide ratios (Figure 7d,e).[81] This change is attributed to the disparity in ionic radius between iodide and bromide, favoring the occupation of iodide in basal or apical positions with different blending ratios. Owing to the different electronegativity, the occupancy of different halogen anions results in alterations within the hydrogen bonding environment, consequently impacting the orientation of organic ligands, as depicted in Figure 7f. This study additionally highlights that the blending of halides contributes to increased structural instability within octahedral layers, proposing a potential method for structural design aimed at amplifying spin-splitting effects.

4. PERSPECTIVE AND OUTLOOK

In the previous section, we reviewed the chemical strategies to manipulate the spin-splitting by rationally designing the ligand structure, dimension, and chemical composition of the chiral perovskite. The asymmetric hydrogen and halogen bonds between the organic and inorganic sublattice play critical roles in the symmetry breaking, which manifests in structural indicator $\Delta\beta$ and further affects α. Details are summarized in Table 1. The chiral ligands modulate the band-splitting from the molecular level of structures, steric hindrance, and specific interactions. First, tail groups-induced intermolecular interaction, for example, the $\pi-\pi$ interactions in conjugated ligands, will enhance the inversion symmetry breaking on achiral parts. It can be found in Table 1 that NEA$^+$ with a larger π-conjugated skeleton will lead to a larger $\Delta\beta$ and band-splitting than MBA$^+$. Second, the steric hindrance effect also contributes to the inorganic lattice distortion since it will lead to discrepancy in the penetration depth of amine groups. Moreover, the functional groups including halogens, hydroxyl groups, and nitro groups will introduce halogen interaction and some other effects like dipole moment, benefiting the symmetry breaking. The functionalized ligand-based chiral perovskite usually enjoys a larger $\Delta\beta$ and α by comparing (S-4-NO$_2$-MBA)$_2$PbBr$_4$ and (R-4-Cl-MBA)$_2$PbBr$_4$ with (S-MBA)$_2$PbI$_4$. The interplay between the dimensions and symmetry breaking is also an essential part of lattice distortion. 1D phases with a larger share of chiral ligands are demonstrated to promote the efficiency of chirality transfer; 2D ACI and DJ phases are predicted to exhibit large lattice distortion while still underexplored due to the limitation of suitable chemical ligands. Apart from the refined design of the ligand structure and dimensions, the chemical composition within the inorganic layers also enriches the distortion motifs. Chiral perovskite with smaller metal centers including Cu^{2+}, Ge^{2+}, and Sb^{3+} will involve the stereochemical expression of ns^2 electrons (SE-NSEP).[50,82,83] The expression of ns^2 lone pair electrons will induce some novel intraoctahedra distortion including the Jahn-teller effect, atom displacement, and bond disproportion, which may engender synergetic ferroelectric and chiral properties.[84,85] The halide component also contributes to the lattice distortion, since the radius and electronegativity difference will give rise to the local residual strain and propagate in the inorganic lattice. To further develop the functionality of chiral perovskites, 3D chiral perovskites are proven advantageous with smaller exciton binding energy and larger charge conductivity, which would benefit the charge-based spintronic devices. Therefore, developing some geometrically suitable chiral ligands to form chiral 3D perovskites under structural constraints could motivate rational material design. So far, the theoretical studies have proved the possibility of 3D chiral perovskite with the smallest chiral ligands such as CHFClNH$_3^+$ or CHDFNH$_3^+$. The experimental studies urgently need to be integrated with calculation results to scrutinize the substantial spin-splitting effect that lies in the electronic structure of 3D chiral perovskite.[86,87]

As the research investigation moves forward, tremendous opportunities and challenges will emerge in terms of material design and device application. In the following discussion, we envision some prospects, including synthesis, characterization, and spintronics applications, to fully exploit the potential of chiral perovskite.

(1) *Controlled crystallization and synthesis process*: To dig into the crystal and electronic structure versatility of chiral perovskite, more complex chiral perovskite systems with modulated spin-splitting can pose issues for the synthesis of high-quality single crystals and films. Therefore, proper synthetic strategies will benefit the rational design of chiral perovskite with tunable crystal and electronic structure. Chiral perovskite single crystals are widely reported with stronger chirality than polycrystal films and powders, owing to their periodic structure and low trap

https://doi.org/10.1021/jacsau.3c00835
JACS Au 2024, 4, 1263−1277

densities. Thus, high-quality chiral perovskite single crystal is an integral part of advancing the studies in crystal structure and band-splitting. Currently, the general synthetic strategies of chiral perovskite single crystal include aqueous synthesis, cooling crystallization, anti-solvent vapor-assisted crystallization, slow evaporation, and nucleation-mediated crystallization.[88] Further efforts are needed to prepare the chiral perovskite with various compositions and crystal phases by intentionally engineering the reactants and solutions. To exploit the practical device applications, the deposition of high-quality thin film preserving single crystal properties also remains challenging. It is essential to control the crystallization kinetics of the chiral perovskite to form a long-range ordered structure. Additionally, various ligand-dependent crystallization with predicted crystal phase and structure is required for further promoting the structure-induced band-splitting.

(2) *In-depth structure−property relationships:* From a material perspective, it is important to mention that chirality transfer does not guarantee the existence of the spin-splitting effect. Therefore, it is crucial to emphasize the necessity of examining the structural asymmetry of all chiral perovskite compounds carefully. Moreover, experimental evidence to corroborate the existence of spin-splitting effect within characteristic crystallographic structures is urgently needed to confirm the structure−property relationship in chiral perovskite. The first direct evidence of Rashba splitting is revealed by angle-resolved photoemission spectroscopy (ARPES), which presents information on the dispersion of band structure.[89] To gain more detailed insight into nanoscale variations in symmetry breaking, scanning tunneling microscopy is employed to image the octahedra tilting on the surface;[69] circular-polarization resolved pump−probe microscopy has been developed to link the spatially resolved propagation of spin currents and the structural inhomogeneity in perovskite films.[90] Developing systematic characterization measurements to study the crystallographic and electronic structure will pave the way for establishing a refined structure−property relationship.[80] In-depth studies of lattice symmetry, band structure, and spin-selectivity in electronic transport within various chiral perovskite systems are also recommended to boost the development of chiro-spintronic devices.[44]

(3) *Spintronics applications*: Multifunctional chiral perovskite systems with the combination of semiconducting, chiroptical, and spin-dependent properties present intriguing prospects. Developing more effective methods to manipulate spin-splitting could significantly advance the integration of spin signals into conventional optical communication systems.[61,91,92] Nonetheless, understanding the diverse mechanisms underlying device functionalities, including relaxation dynamics intertwined with spin-splitting effects during device operation, remains a challenge. A comprehensive exploration of both material and device operational principles is vital to propel advancements in spintronics.

AUTHOR INFORMATION

Corresponding Author

Mingjian Yuan − *State Key Laboratory of Advanced Chemical Power Sources, Key Laboratory of Advanced Energy Materials Chemistry (Ministry of Education), Frontiers Science Center for New Organic Matter, College of Chemistry, Nankai University, Tianjin 300071, P. R. China; Haihe Laboratory of Sustainable Chemical Transformations, Tianjin 300051, P. R. China;* orcid.org/0000-0002-2790-9172; Email: yuanmj@nankai.edu.cn

Authors

Zijin Ding − *State Key Laboratory of Advanced Chemical Power Sources, Key Laboratory of Advanced Energy Materials Chemistry (Ministry of Education), Frontiers Science Center for New Organic Matter, College of Chemistry, Nankai University, Tianjin 300071, P. R. China*

Quanlin Chen − *State Key Laboratory of Advanced Chemical Power Sources, Key Laboratory of Advanced Energy Materials Chemistry (Ministry of Education), Frontiers Science Center for New Organic Matter, College of Chemistry, Nankai University, Tianjin 300071, P. R. China*

Yuanzhi Jiang − *State Key Laboratory of Advanced Chemical Power Sources, Key Laboratory of Advanced Energy Materials Chemistry (Ministry of Education), Frontiers Science Center for New Organic Matter, College of Chemistry, Nankai University, Tianjin 300071, P. R. China;* orcid.org/0000-0001-6580-9255

Complete contact information is available at: https://pubs.acs.org/10.1021/jacsau.3c00835

Author Contributions

All authors have given approval to the final version of the manuscript.

Notes

The authors declare no competing financial interest.

ACKNOWLEDGMENTS

This work is financially supported by the National Science Fund for Distinguished Young Scholars (No. T2225024) and the National Key Research and Development Program of China(2022YFE0201500). The authors acknowledge financial support from the National Natural Science Foundation of China (No. 62261160389).

REFERENCES

(1) Saparov, B.; Mitzi, D. B. Organic-Inorganic Perovskites: Structural Versatility for Functional Materials Design. *Chem. Rev.* **2016**, *116* (7), 4558−4596.

(2) Li, W.; Wang, Z.; Deschler, F.; Gao, S.; Friend, R. H.; Cheetham, A. K. Chemically Diverse and Multifunctional Hybrid Organic-Inorganic Perovskites. *Nat. Rev. Mater.* **2017**, *2* (3), 16099.

(3) Liu, C.; Yang, Y.; Chen, H.; Xu, J.; Liu, A.; Bati, A. S. R.; Zhu, H.; Grater, L.; Hadke, S. S.; Huang, C.; Sangwan, V. K.; Cai, T.; Shin, D.; Chen, L. X.; Hersam, M. C.; Mirkin, C. A.; Chen, B.; Kanatzidis, M. G.; Sargent, E. H. Bimolecularly Passivated Interface Enables Efficient and Stable Inverted Perovskite Solar Cells. *Science* **2023**, *382* (6672), 810−815.

(4) Jiang, Y.; Sun, C.; Xu, J.; Li, S.; Cui, M.; Fu, X.; Liu, Y.; Liu, Y.; Wan, H.; Wei, K.; Zhou, T.; Zhang, W.; Yang, Y.; Yang, J.; Qin, C.; Gao, S.; Pan, J.; Liu, Y.; Hoogland, S.; Sargent, E. H.; Chen, J.; Yuan, M. Synthesis-on-Substrate of Quantum Dot Solids. *Nature* **2022**, *612* (7941), 679−684.

(5) Jiang, Y.; Wei, K.; Sun, C.; Feng, Y.; Zhang, L.; Cui, M.; Li, S.; Li, W.-D.; Kim, J. T.; Qin, C.; Yuan, M. Unraveling Size-Dependent Ion-Migration for Stable Mixed-Halide Perovskite Light-Emitting Diodes. *Adv. Mater.* **2023**, *35* (39), 2304094.
(6) Long, G.; Sabatini, R.; Saidaminov, M. I.; Lakhwani, G.; Rasmita, A.; Liu, X.; Sargent, E. H.; Gao, W. Chiral-perovskite optoelectronics. *Nat. Rev. Mater.* **2020**, *5* (6), 423−439.
(7) Lu, H.; Vardeny, Z. V.; Beard, M. C. Control of Light, Spin and Charge with Chiral Metal Halide Semiconductors. *Nat. Rev. Chem.* **2022**, *6* (7), 470−485.
(8) Crassous, J.; Fuchter, M. J.; Freedman, D. E.; Kotov, N. A.; Moon, J.; Beard, M. C.; Feldmann, S. Materials for chiral light control. *Nat. Rev. Mater.* **2023**, *8* (6), 365−371.
(9) Morrow, S. M.; Bissette, A. J.; Fletcher, S. P. Transmission of chirality through space and across length scales. *Nat. Nanotechnol.* **2017**, *12* (5), 410−419.
(10) Ma, J.; Wang, H.; Li, D. Recent Progress of Chiral Perovskites: Materials, Synthesis, and Properties. *Adv. Mater.* **2021**, *33* (26), 2008785.
(11) Privitera, A.; Righetto, M.; Cacialli, F.; Riede, M. K. Perspectives of Organic and Perovskite-Based Spintronics. *Adv. Opt. Mater.* **2021**, *9* (14), 2100215.
(12) Kepenekian, M.; Robles, R.; Katan, C.; Sapori, D.; Pedesseau, L.; Even, J. Rashba and Dresselhaus Effects in Hybrid Organic-Inorganic Perovskites: From Basics to Devices. *ACS Nano* **2015**, *9* (12), 11557−11567.
(13) Zhang, X.; Liu, Q.; Luo, J.-W.; Freeman, A. J.; Zunger, A. Hidden Spin Polarization in Inversion-Symmetric Bulk Crystals. *Nat. Phys.* **2014**, *10* (5), 387−393.
(14) Frohna, K.; Deshpande, T.; Harter, J.; Peng, W.; Barker, B. A.; Neaton, J. B.; Louie, S. G.; Bakr, O. M.; Hsieh, D.; Bernardi, M. Inversion Symmetry and Bulk Rashba Effect in Methylammonium Lead Iodide Perovskite Single Crystals. *Nat. Commun.* **2018**, *9* (1), 1829.
(15) Jana, M. K.; Song, R.; Liu, H.; Khanal, D. R.; Janke, S. M.; Zhao, R.; Liu, C.; Valy Vardeny, Z.; Blum, V.; Mitzi, D. B. Organic-to-Inorganic Structural Chirality Transfer in a 2D Hybrid Perovskite and Impact on Rashba-Dresselhaus Spin-Orbit Coupling. *Nat. Commun.* **2020**, *11* (1), 4699.
(16) Ma, S.; Ahn, J.; Moon, J. Chiral Perovskites for Next-Generation Photonics: From Chirality Transfer to Chiroptical Activity. *Adv. Mater.* **2021**, *33* (47), 2005760.
(17) Stranks, S. D.; Plochocka, P. The Influence of the Rashba Effect. *Nat. Mater.* **2018**, *17* (5), 381−382.
(18) Ma, S.; Jung, Y.-K.; Ahn, J.; Kyhm, J.; Tan, J.; Lee, H.; Jang, G.; Lee, C. U.; Walsh, A.; Moon, J. Elucidating The Origin of Chiroptical Activity in Chiral 2D Perovskites through Nano-Confined Growth. *Nat. Commun.* **2022**, *13* (1), 3259.
(19) Yan, L.; Jana, M. K.; Sercel, P. C.; Mitzi, D. B.; You, W. Alkyl-Aryl Cation Mixing in Chiral 2D Perovskites. *J. Am. Chem. Soc.* **2021**, *143* (43), 18114−18120.
(20) Hu, Y.; Florio, F.; Chen, Z.; Phelan, W. A.; Siegler, M. A.; Zhou, Z.; Guo, Y.; Hawks, R.; Jiang, J.; Feng, J.; Zhang, L.; Wang, B.; Wang, Y.; Gall, D.; Palermo, E. F.; Lu, Z.; Sun, X.; Lu, T.-M.; Zhou, H.; Ren, Y.; Wertz, E.; Sundararaman, R.; Shi, J. A Chiral Switchable Photovoltaic Ferroelectric 1D Perovskite. *Sci. Adv.* **2020**, *6* (9), No. eaay4213.
(21) Fan, C.-C.; Han, X.-B.; Liang, B.-D.; Shi, C.; Miao, L.-P.; Chai, C.-Y.; Liu, C.-D.; Ye, Q.; Zhang, W. Chiral Rashba Ferroelectrics for Circularly Polarized Light Detection. *Adv. Mater.* **2022**, *34* (51), 2204119.
(22) Jana, M. K.; Song, R.; Xie, Y.; Zhao, R.; Sercel, P. C.; Blum, V.; Mitzi, D. B. Structural Descriptor for Enhanced Spin-Splitting in 2D Hybrid Perovskites. *Nat. Commun.* **2021**, *12* (1), 4982.
(23) Lin, J.-T.; Chen, D.-G.; Yang, L.-S.; Lin, T.-C.; Liu, Y.-H.; Chao, Y.-C.; Chou, P.-T.; Chiu, C.-W. Tuning the Circular Dichroism and Circular Polarized Luminescence Intensities of Chiral 2D Hybrid Organic-Inorganic Perovskites through Halogenation of the Organic Ions. *Angew. Chem., Int. Ed.* **2021**, *60* (39), 21434−21440.
(24) Gao, J.-X.; Zhang, W.-Y.; Wu, Z.-G.; Zheng, Y.-X.; Fu, D.-W. Enantiomorphic Perovskite Ferroelectrics with Circularly Polarized Luminescence. *J. Am. Chem. Soc.* **2020**, *142* (10), 4756−4761.
(25) Peng, Y.; Yao, Y.; Li, L.; Wu, Z.; Wang, S.; Luo, J. White-Light Emission in a Chiral One-Dimensional Organic-Inorganic Hybrid Perovskite. *J. Mater. Chem. C* **2018**, *6* (22), 6033−6037.
(26) He, T.; Li, J.; Li, X.; Ren, C.; Luo, Y.; Zhao, F.; Chen, R.; Lin, X.; Zhang, J. Spectroscopic Studies of Chiral Perovskite Nanocrystals. *Appl. Phys. Lett.* **2017**, *111* (15), 151102.
(27) Sirenko, V. Y.; Kucheriv, O. I.; Naumova, D. D.; Fesych, I. V.; Linnik, R. P.; Dascălu, I.-A.; Shova, S.; Fritsky, I. O.; Gural'skiy, I. y. A. Chiral Organic-Inorganic Lead Halide Perovskites Based on α-Alanine. *New J. Chem.* **2021**, *45* (28), 12606−12612.
(28) Chen, W.; Zhang, S.; Zhou, M.; Zhao, T.; Qin, X.; Liu, X.; Liu, M.; Duan, P. Two-Photon Absorption-Based Upconverted Circularly Polarized Luminescence Generated in Chiral Perovskite Nanocrystals. *J. Phys. Chem. Lett.* **2019**, *10* (12), 3290−3295.
(29) Stoumpos, C. C.; Kanatzidis, M. G. The Renaissance of Halide Perovskites and Their Evolution as Emerging Semiconductors. *Acc. Chem. Res.* **2015**, *48* (10), 2791−2802.
(30) Chakraborty, S.; Nazeeruddin, M. K. The Status Quo of Rashba Phenomena in Organic-Inorganic Hybrid Perovskites. *J. Phys. Chem. Lett.* **2021**, *12* (1), 361−367.
(31) Zheng, F.; Tan, L. Z.; Liu, S.; Rappe, A. M. Rashba Spin-Orbit Coupling Enhanced Carrier Lifetime in $CH_3NH_3PbI_3$. *Nano Lett.* **2015**, *15* (12), 7794−7800.
(32) Long, G.; Jiang, C.; Sabatini, R.; Yang, Z.; Wei, M.; Quan, L. N.; Liang, Q.; Rasmita, A.; Askerka, M.; Walters, G.; Gong, X.; Xing, J.; Wen, X.; Quintero-Bermudez, R.; Yuan, H.; Xing, G.; Wang, X. R.; Song, D.; Voznyy, O.; Zhang, M.; Hoogland, S.; Gao, W.; Xiong, Q.; Sargent, E. H. Spin Control in Reduced-Dimensional Chiral Perovskites. *Nat. Photonics* **2018**, *12* (9), 528−533.
(33) Mao, L.; Stoumpos, C. C.; Kanatzidis, M. G. Two-Dimensional Hybrid Halide Perovskites: Principles and Promises. *J. Am. Chem. Soc.* **2019**, *141* (3), 1171−1190.
(34) Bychkov, Y. A.; Rashba, É. I. Properties of a 2D Electron Gas with Lifted Spectral Degeneracy. *J. Exp. Theor. Phys.* **1984**, *39* (2), 78.
(35) Manchon, A.; Koo, H. C.; Nitta, J.; Frolov, S. M.; Duine, R. A. New Perspectives for Rashba Spin-Orbit Coupling. *Nat. Mater.* **2015**, *14* (9), 871−882.
(36) Wolf, S. A.; Awschalom, D. D.; Buhrman, R. A.; Daughton, J. M.; von Molnár, S.; Roukes, M. L.; Chtchelkanova, A. Y.; Treger, D. M. Spintronics: A Spin-Based Electronics Vision for the Future. *Science* **2001**, *294* (5546), 1488−1495.
(37) Maurer, B.; Vorwerk, C.; Draxl, C. Rashba and Dresselhaus Effects in Two-Dimensional Pb-I-Based Perovskites. *Phys. Rev. B* **2022**, *105* (15), 155149.
(38) Kepenekian, M.; Even, J. Rashba and Dresselhaus Couplings in Halide Perovskites: Accomplishments and Opportunities for Spintronics and Spin-Orbitronics. *J. Phys. Chem. Lett.* **2017**, *8* (14), 3362−3370.
(39) Dresselhaus, G. J. P. R. Spin-Orbit Coupling Effects in Zinc Blende Structures. *Phys. Rev.* **1955**, *100* (2), 580.
(40) McKechnie, S.; Frost, J. M.; Pashov, D.; Azarhoosh, P.; Walsh, A.; van Schilfgaarde, M. Dynamic Symmetry Breaking and Spin Splitting in Metal Halide Perovskites. *Phys. Rev. B* **2018**, *98* (8), 085108.
(41) Kurebayashi, H.; Sinova, J.; Fang, D.; Irvine, A. C.; Skinner, T. D.; Wunderlich, J.; Novák, V.; Campion, R. P.; Gallagher, B. L.; Vehstedt, E. K.; Zârbo, L. P.; Výborný, K.; Ferguson, A. J.; Jungwirth, T. An Antidamping Spin-Orbit Torque Originating from The Berry Curvature. *Nat. Nanotechnol.* **2014**, *9* (3), 211−217.
(42) Zheng, C.; Yu, S.; Rubel, O. J. P. R. M. Structural Dynamics in Hybrid Halide Perovskites: Bulk Rashba Splitting, Spin Texture, and Carrier Localization. *Phys. Rev. Mater.* **2018**, *2* (11), 114604.
(43) Liu, X.; Chanana, A.; Huynh, U.; Xue, F.; Haney, P.; Blair, S.; Jiang, X.; Vardeny, Z. V. Circular Photogalvanic Spectroscopy of Rashba Splitting in 2D Hybrid Organic-Inorganic Perovskite Multiple Quantum Wells. *Nat. Commun.* **2020**, *11* (1), 323.

https://doi.org/10.1021/jacsau.3c00835
JACS Au 2024, 4, 1263−1277

(44) Abhervé, A.; Mercier, N.; Kumar, A.; Das, T. K.; Even, J.; Katan, C.; Kepenekian, M. Chirality Versus Symmetry: Electron's Spin Selectivity in Nonpolar Chiral Lead-Bromide Perovskites. *Adv. Mater.* **2023**, *35* (51), 2305784.
(45) Dolamic, I.; Knoppe, S.; Dass, A.; Bürgi, T. First Enantioseparation and Circular Dichroism Spectra of Au_{38} Clusters Protected by Achiral Ligands. *Nat. Commun.* **2012**, *3* (1), 798.
(46) Ben-Moshe, A.; Wolf, S. G.; Sadan, M. B.; Houben, L.; Fan, Z.; Govorov, A. O.; Markovich, G. Enantioselective Control of Lattice and Shape Chirality in Inorganic Nanostructures Using Chiral Biomolecules. *Nat. Commun.* **2014**, *5* (1), 4302.
(47) Zhou, Y.; Yang, M.; Sun, K.; Tang, Z.; Kotov, N. A. Similar Topological Origin of Chiral Centers in Organic and Nanoscale Inorganic Structures: Effect of Stabilizer Chirality on Optical Isomerism and Growth of CdTe Nanocrystals. *J. Am. Chem. Soc.* **2010**, *132* (17), 6006−6013.
(48) Tohgha, U.; Deol, K. K.; Porter, A. G.; Bartko, S. G.; Choi, J. K.; Leonard, B. M.; Varga, K.; Kubelka, J.; Muller, G.; Balaz, M. Ligand Induced Circular Dichroism and Circularly Polarized Luminescence in CdSe Quantum Dots. *ACS Nano* **2013**, *7* (12), 11094−11102.
(49) Liu, H.-Y.; Zhang, H.-Y.; Chen, X.-G.; Xiong, R.-G. Molecular Design Principles for Ferroelectrics: Ferroelectrochemistry. *J. Am. Chem. Soc.* **2020**, *142* (36), 15205−15218.
(50) Fu, Y.; Jin, S.; Zhu, X. Y. Stereochemical expression of ns^2 electron pairs in metal halide perovskites. *Nat. Rev. Chem.* **2021**, *5* (12), 838−852.
(51) Du, K.-z.; Tu, Q.; Zhang, X.; Han, Q.; Liu, J.; Zauscher, S.; Mitzi, D. B. Two-Dimensional Lead(II) Halide-Based Hybrid Perovskites Templated by Acene Alkylamines: Crystal Structures, Optical Properties, and Piezoelectricity. *Inorg. Chem.* **2017**, *56* (15), 9291−9302.
(52) Amat, A.; Mosconi, E.; Ronca, E.; Quarti, C.; Umari, P.; Nazeeruddin, M. K.; Grätzel, M.; De Angelis, F. Cation-Induced Band-Gap Tuning in Organohalide Perovskites: Interplay of Spin-Orbit Coupling and Octahedra Tilting. *Nano Lett.* **2014**, *14* (6), 3608−3616.
(53) Bhattacharya, S.; Kanai, Y. Spin-Orbit-Coupling-Induced Band Splitting in Two-Dimensional Hybrid Organic-Inorganic Perovskites: Importance of Organic Cations. *Phys. Rev. Mater.* **2023**, *7* (5), 055001.
(54) Lu, H.; Xiao, C.; Song, R.; Li, T.; Maughan, A. E.; Levin, A.; Brunecky, R.; Berry, J. J.; Mitzi, D. B.; Blum; Beard, M. C. Highly Distorted Chiral Two-Dimensional Tin Iodide Perovskites for Spin-Polarized Charge Transport. *J. Am. Chem. Soc.* **2020**, *142* (30), 13030−13040.
(55) Ishii, A.; Miyasaka, T. Direct detection of circular polarized light in helical 1D perovskite-based photodiode. *Sci. Adv.* **2020**, *6* (46), No. eabd3274.
(56) Zhang, Y.; Sun, M.; Zhou, N.; Huang, B.; Zhou, H. Electronic Tunability and Mobility Anisotropy of Quasi-2D Perovskite Single Crystals with Varied Spacer Cations. *J. Phys. Chem. Lett.* **2020**, *11* (18), 7610−7616.
(57) Xiao, J.; Zheng, H.; Wang, R.; Wang, Y.; Hou, S. Spin-Polarized Excitons and Charge Carriers in Chiral Metal Halide Semiconductors. *J. Mater. Chem. A* **2022**, *10* (37), 19367−19386.
(58) Jiang, S.; Song, Y.; Kang, H.; Li, B.; Yang, K.; Xing, G.; Yu, Y.; Li, S.; Zhao, P.; Zhang, T. Ligand Exchange Strategy to Achieve Chiral Perovskite Nanocrystals with a High Photoluminescence Quantum Yield and Regulation of the Chiroptical Property. *ACS Appl. Mater. Interfaces* **2022**, *14* (2), 3385−3394.
(59) Son, J.; Ma, S.; Jung, Y.-K.; Tan, J.; Jang, G.; Lee, H.; Lee, C. U.; Lee, J.; Moon, S.; Jeong, W.; Walsh, A.; Moon, J. Unraveling Chirality Transfer Mechanism by Structural Isomer-Derived Hydrogen Bonding Interaction in 2D Chiral Perovskite. *Nat. Commun.* **2023**, *14* (1), 3124.
(60) Schmitt, T.; Bourelle, S.; Tye, N.; Soavi, G.; Bond, A. D.; Feldmann, S.; Traore, B.; Katan, C.; Even, J.; Dutton, S. E.; Deschler, F. Control of Crystal Symmetry Breaking with Halogen-Substituted Benzylammonium in Layered Hybrid Metal-Halide Perovskites. *J. Am. Chem. Soc.* **2020**, *142* (11), 5060−5067.
(61) Liu, S.; Kepenekian, M.; Bodnar, S.; Feldmann, S.; Heindl, M. W.; Fehn, N.; Zerhoch, J.; Shcherbakov, A.; Pöthig, A.; Li, Y.; Paetzold, U. W.; Kartouzian, A.; Sharp, I. D.; Katan, C.; Even, J.; Deschler, F. Bright Circularly Polarized Photoluminescence in Chiral Layered Hybrid Lead-Halide Perovskites. *Sci. Adv.* **2023**, *9* (35), No. eadh5083.
(62) Wei, Q.; Zhang, Q.; Xiang, L.; Zhang, S.; Liu, J.; Yang, X.; Ke, Y.; Ning, Z. Giant Spin Splitting in Chiral Perovskites Based on Local Electrical Field Engineering. *J. Phys. Chem. Lett.* **2021**, *12* (28), 6492−6498.
(63) Xue, J.; Huang, Y.; Liu, Y.; Chen, Z.; Sung, H. H. Y.; Williams, I. D.; Zhu, Z.; Mao, L.; Chen, X.; Lu, H. Rashba Band Splitting and Bulk Photovoltaic Effect Induced by Halogen Bonds in Hybrid Layered Perovskites. *Angew. Chem., Int. Ed.* **2023**, *62* (29), No. e202304486.
(64) Lee, C. U.; Ma, S.; Ahn, J.; Kyhm, J.; Tan, J.; Lee, H.; Jang, G.; Park, Y. S.; Yun, J.; Lee, J.; Son, J.; Park, J.-S.; Moon, J. Tailoring the Time-Averaged Structure for Polarization-Sensitive Chiral Perovskites. *J. Am. Chem. Soc.* **2022**, *144* (35), 16020−16033.
(65) Xie, Y.; Morgenstein, J.; Bobay, B. G.; Song, R.; Caturello, N. A. M. S.; Sercel, P. C.; Blum, V.; Mitzi, D. B. Chiral Cation Doping for Modulating Structural Symmetry of 2D Perovskites. *J. Am. Chem. Soc.* **2023**, *145* (32), 17831−17844.
(66) Zhu, T.; Wu, H.; Ji, C.; Zhang, X.; Peng, Y.; Yao, Y.; Ye, H.; Weng, W.; Lin, W.; Luo, J. Polar Photovoltaic Effect in Chiral Alternating Cations Intercalation-Type Perovskites Driving Self-Powered Ultraviolet Circularly Polarized Light Detection. *Adv. Opt. Mater.* **2022**, *10* (15), 2200146.
(67) Zhou, B.; Liang, L.; Ma, J.; Li, J.; Li, W.; Liu, Z.; Li, H.; Chen, R.; Li, D. Thermally Assisted Rashba Splitting and Circular Photogalvanic Effect in Aqueously Synthesized 2D Dion-Jacobson Perovskite Crystals. *Nano Lett.* **2021**, *21* (11), 4584−4591.
(68) Leng, K.; Li, R.; Lau, S. P.; Loh, K. P. Ferroelectricity and Rashba effect in 2D organic-inorganic hybrid perovskites. *Trends Chem.* **2021**, *3* (9), 716−732.
(69) Shao, Y.; Gao, W.; Yan, H.; Li, R.; Abdelwahab, I.; Chi, X.; Rogée, L.; Zhuang, L.; Fu, W.; Lau, S. P.; Yu, S. F.; Cai, Y.; Loh, K. P.; Leng, K. Unlocking Surface Octahedral Tilt in Two-Dimensional Ruddlesden-Popper Perovskites. *Nat. Commun.* **2022**, *13* (1), 138.
(70) Chen, C.; Gao, L.; Gao, W.; Ge, C.; Du, X.; Li, Z.; Yang, Y.; Niu, G.; Tang, J. Circularly Polarized Light Detection Using Chiral Hybrid Perovskite. *Nat. Commun.* **2019**, *10* (1), 1927.
(71) Zhu, T.; Weng, W.; Ji, C.; Zhang, X.; Ye, H.; Yao, Y.; Li, X.; Li, J.; Lin, W.; Luo, J. Chain-to-Layer Dimensionality Engineering of Chiral Hybrid Perovskites to Realize Passive Highly Circular-Polarization-Sensitive Photodetection. *J. Am. Chem. Soc.* **2022**, *144* (39), 18062−18068.
(72) Li, J.; Li, J.; Liu, R.; Tu, Y.; Li, Y.; Cheng, J.; He, T.; Zhu, X. Autonomous Discovery of Optically Active Chiral Inorganic Perovskite Nanocrystals through an Intelligent Cloud Lab. *Nat. Commun.* **2020**, *11* (1), 2046.
(73) Kim, Y.-H.; Song, R.; Hao, J.; Zhai, Y.; Yan, L.; Moot, T.; Palmstrom, A. F.; Brunecky, R.; You, W.; Berry, J. J.; Blackburn, J. L.; Beard, M. C.; Blum, V.; Luther, J. M. The Structural Origin of Chiroptical Properties in Perovskite Nanocrystals with Chiral Organic Ligands. *Adv. Funct. Mater.* **2022**, *32* (25), 2200454.
(74) Ye, C.; Jiang, J.; Zou, S.; Mi, W.; Xiao, Y. Core-Shell Three-Dimensional Perovskite Nanocrystals with Chiral-Induced Spin Selectivity for Room-Temperature Spin Light-Emitting Diodes. *J. Am. Chem. Soc.* **2022**, *144* (22), 9707−9714.
(75) Odenthal, P.; Talmadge, W.; Gundlach, N.; Wang, R.; Zhang, C.; Sun, D.; Yu, Z.-G.; Valy Vardeny, Z.; Li, Y. S. Spin-Polarized Exciton Quantum Beating in Hybrid Organic-Inorganic Perovskites. *Nat. Phys.* **2017**, *13* (9), 894−899.
(76) Li, D.; Liu, X.; Wu, W.; Peng, Y.; Zhao, S.; Li, L.; Hong, M.; Luo, J. Chiral Lead-Free Hybrid Perovskites for Self-Powered Circularly Polarized Light Detection. *Angew. Chem., Int. Ed.* **2021**, *60* (15), 8415−8418.
(77) Stroppa, A.; Di Sante, D.; Barone, P.; Bokdam, M.; Kresse, G.; Franchini, C.; Whangbo, M.-H.; Picozzi, S. Tunable Ferroelectric Polarization and Its Interplay with Spin-Orbit Coupling in Tin Iodide Perovskites. *Nat. Commun.* **2014**, *5* (1), 5900.
(78) Banerjee, A.; Chakraborty, S.; Ahuja, R. Rashba Triggered Electronic and Optical Properties Tuning in Mixed Cation-Mixed

https://doi.org/10.1021/jacsau.3c00835
JACS Au 2024, 4, 1263−1277

Halide Hybrid Perovskites. *ACS Appl. Energy Mater.* **2019**, *2* (10), 6990−6997.
(79) Shi, R.; Pi, J.; Chu, D.; Jia, B.; Zhao, Z.; Hao, J.; Zhang, X.; Dong, X.; Liang, Y.; Zhang, Y.; Liu, Y.; Liu, S. Promoting Band Splitting through Symmetry Breaking in Inorganic Halide Perovskite Single Crystals for High-Sensitivity X-ray Detection. *ACS Energy Lett.* **2023**, *8* (11), 4836−4847.
(80) Lafalce, E.; Amerling, E.; Yu, Z.-G.; Sercel, P. C.; Whittaker-Brooks, L.; Vardeny, Z. V. Rashba Splitting in Organic-Inorganic Lead-Halide Perovskites Revealed through Two-Photon Absorption Spectroscopy. *Nat. Commun.* **2022**, *13* (1), 483.
(81) Ahn, J.; Ma, S.; Kim, J.-Y.; Kyhm, J.; Yang, W.; Lim, J. A.; Kotov, N. A.; Moon, J. Chiral 2D Organic Inorganic Hybrid Perovskite with Circular Dichroism Tunable Over Wide Wavelength Range. *J. Am. Chem. Soc.* **2020**, *142* (9), 4206−4212.
(82) Morteza Najarian, A.; Dinic, F.; Chen, H.; Sabatini, R.; Zheng, C.; Lough, A.; Maris, T.; Saidaminov, M. I.; García de Arquer, F. P.; Voznyy, O.; Hoogland, S.; Sargent, E. H. Homomeric Chains of Intermolecular Bonds Scaffold Octahedral Germanium Perovskites. *Nature* **2023**, *620* (7973), 328−335.
(83) Yao, L.; Niu, G.; Li, J.; Gao, L.; Luo, X.; Xia, B.; Liu, Y.; Du, P.; Li, D.; Chen, C.; Zheng, Y.; Xiao, Z.; Tang, J. Circularly Polarized Luminescence from Chiral Tetranuclear Copper(I) Iodide Clusters. *J. Phys. Chem. Lett.* **2020**, *11* (4), 1255−1260.
(84) Gui, D.; Ji, L.; Muhammad, A.; Li, W.; Cai, W.; Li, Y.; Li, X.; Wu, X.; Lu, P. Jahn-Teller Effect on Framework Flexibility of Hybrid Organic-Inorganic Perovskites. *J. Phys. Chem. Lett.* **2018**, *9* (4), 751−755.
(85) Wang, Z.; Malyi, O. I.; Zhao, X.; Zunger, A. Mass Enhancement in *3d* and *s-p* Perovskites from Symmetry Breaking. *Phys. Rev. B* **2021**, *103* (16), 165110.
(86) Ye, H.-Y.; Tang, Y.-Y.; Li, P.-F.; Liao, W.-Q.; Gao, J.-X.; Hua, X.-N.; Cai, H.; Shi, P.-P.; You, Y.-M.; Xiong, R.-G. Metal-Free Three-Dimensional Perovskite Ferroelectrics. *Science* **2018**, *361* (6398), 151−155.
(87) Huang, S.; Huang, P.; Wang, L.; Han, J.; Chen, Y.; Zhong, H. Halogenated-Methylammonium Based 3D Halide Perovskites. *Adv. Mater.* **2019**, *31* (42), 1903830.
(88) Ma, J.; Wang, H.; Li, D. Recent Progress of Chiral Perovskites: Materials, Synthesis, and Properties. *Adv. Mater.* **2021**, *33* (26), 2008785.
(89) Ma, J.; Fang, C.; Chen, C.; Jin, L.; Wang, J.; Wang, S.; Tang, J.; Li, D. Chiral 2D Perovskites with a High Degree of Circularly Polarized Photoluminescence. *ACS Nano* **2019**, *13* (3), 3659−3665.
(90) Ashoka, A.; Nagane, S.; Strkalj, N.; Sharma, A.; Roose, B.; Sneyd, A. J.; Sung, J.; MacManus-Driscoll, J. L.; Stranks, S. D.; Feldmann, S.; Rao, A. Local Symmetry Breaking Drives Picosecond Spin Domain Formation in Polycrystalline Halide Perovskite Films. *Nat. Mater.* **2023**, *22* (8), 977−984.
(91) Zhao, Y.; Qiu, Y.; Feng, J.; Zhao, J.; Chen, G.; Gao, H.; Zhao, Y.; Jiang, L.; Wu, Y. Chiral 2D-Perovskite Nanowires for Stokes Photodetectors. *J. Am. Chem. Soc.* **2021**, *143* (22), 8437−8445.
(92) Kim, Y.-H.; Zhai, Y.; Lu, H.; Pan, X.; Xiao, C.; Gaulding, E. A.; Harvey, S. P.; Berry, J. J.; Vardeny, Z. V.; Luther, J. M.; Beard, M. C. Chiral-Induced Spin Selectivity Enables a Room-Temperature Spin Light-Emitting Diode. *Science* **2021**, *371* (6534), 1129−1133.

https://doi.org/10.1021/jacsau.3c00835
JACS Au 2024, 4, 1263−1277